Polarization fluctuations in the perovskite-structured ferroelectric AgNbO_{3}

Hiroki Moriwake, Ayako Konishi, Takafumi Ogawa, Craig A. J. Fisher, Akihide Kuwabara, Kazuki Shitara, and Desheng Fu

Phys. Rev. B **97**, 224104 — Published 20 June 2018

DOI: 10.1103/PhysRevB.97.224104

Polarization fluctuations in perovskite-structured ferroelectric $AgNbO_3$

Hiroki Moriwake,[1,2*] Ayako Konishi,[1,2] Takafumi Ogawa,[1] Craig A. J. Fisher,[1] Akihide Kuwabara,[1,2] Kazuki Shitara,[1,2] and Desheng Fu[3]

[1]Nanostructures Research Laboratory, Japan Fine Ceramics Center, Nagoya, 456-8587, Japan
[2]Center for Materials Research by Information Integration (CMI[2]), National Institute for Materials Science, 1-2-1 Sengen, Tsukuba, Ibaraki 305-0047, Japan
[3]Department of Electronics & Materials Sciences, Shizuoka University, Hamamatsu, 432-8561, Japan

Perovskite-structured $AgNbO_3$ is a promising lead-free ferroelectric material that at room temperature exhibits weak ferroelectric behavior with a large polarization under an applied electric field. Here we report first-principles molecular dynamics (FPMD) simulations of monocrystalline $AgNbO_3$ over a range of temperatures to examine the microscopic polarization switching mechanism. Polarization switching is found to occur at temperatures around 200 K and above; regardless of whether the simulations commence from the antiferroelectric *Pbcm* structure or ferroelectric $Pmc2_1$ structure, above 200 K the crystal fluctuates between the two forms. The FPMD are consistent with the coexistence of the two phases at room temperature, which can explain the mixed ferroelectric/antiferroelectric behavior, such as double P-E hysteresis loops, observed experimentally.

Keywords: ferroelectric, $AgNbO_3$, polarization switching, first-principles calculations

1. Introduction

Perovskite-structured silver niobate, $AgNbO_3$, is a promising compound from which lead-free piezoelectrics can be developed to replace lead zirconate titanate, better known as PZT, and similar materials in a range of advanced applications such as thin-film wave guides, laser beam modulators, surface acoustic wave devices, and electrophotography. Since the discovery of weak room-temperature ferroelectric behavior in $AgNbO_3$, high-quality stoichiometric ceramic samples have been synthesized that exhibit a large polarization of 52 $\mu C/cm^2$ after application of a high electric field of 220 kV/cm [1]. Similar to other perovskite niobates, $AgNbO_3$ undergoes a complex series of phase transitions as a function of temperature, pressure, and electric field, and many details about the subtly different ferroelectric (FE) and antiferroelectric (AFE) states are still not well understood, prompting a number of experimental and theoretical studies in recent years [2-10].

X-ray and neutron diffraction analyses by Sciau *et al.* [2] showed that at high temperature $AgNbO_3$ exists as a cubic phase (space group $Pm\bar{3}m$), referred to as the C phase, which transforms to a paraelectric tetragonal phase with $P4/mbm$ symmetry (the T phase) at 852 K. This is followed by transitions to two paraelectric phases with orthorhombic symmetry (space group *Cmcm*), the first at 660 K and the second at 634 K, upon further cooling. These two orthorhombic polymorphs are referred to as O_2 and O_1, respectively.

At 626 K, $AgNbO_3$ undergoes a paraelectric-to-antiferroelectric transition in which the optical axes change from parallel orientation to rhombic orientation. Unlike at high temperature, in the low-temperature regime further phase transitions are diffuse and the different phases difficult to distinguish. Sciau *et al.* [2] concluded that three low-temperature phases form with orthorhombic symmetry (referred to as M_3, M_2, and M_1 in order of decreasing temperature stability range) assigning space group *Pbcm* to all three. Under zero electric field, the room-temperature M_1 phase was found to

exhibit a remanent polarization of ~0.05 μC/cm^2, even though the assigned space group is centrosymmetric. It was suggested that local structural defects (e.g., cation disorder or vacancy clustering) were responsible for the weak ferroelectricity. Subsequently, based on detailed neutron diffraction experiments, Yashima *et al.* [4,5] and Chang *et al.* [6] re-assigned the M_1 phase to space group $Pmc2_1$, a non-centrosymmetric space group consistent with the weak FE behavior. An interesting feature of the reported crystal structure is that it is ferrielectric, with antiparallel Nb-O and Ag-O displacements of different magnitudes producing a theoretical polarization value of 3.7 μC/cm^2, rather than a fully ferroelectric structure in which all Nb-O displacements of equal magnitude are aligned in the same direction, as are Ag-O displacements.

By examining the dielectric and FE behavior of $AgNbO_3$ at temperatures below 298 K using a variety of techniques, Zhang *et al.* [11] recently identified another FE phase below 250 K, which they refer to as M_0. They recorded a slightly higher remanent polarization (2.4 μC/cm^2) than the M_1 phase (0.041 μC/cm^2), and attributed the increased ferroelectricity to reduction in the AFE ordering of Ag atoms, although they did not determine the precise crystal structure.

First-principles calculations have proven to be powerful tools for examining FE-AFE phase transitions because they allow crystal structures to be studied in isolation under well-defined conditions [12]. For example, by analyzing soft phonon modes in phonon dispersion curves and calculating relative lattice energies, we have identified phase transition sequences and their corresponding microscopic mechanisms for a range of perovskite materials such as $BaTiO_3$, $CdTiO_3$, and $Cd_{1-x}Ca_xTiO_3$.[7-9]

Early efforts to understand the ferroelectric behavior of $AgNbO_3$ from a theoretical point of view were reported by Griberg and Rappe [13], who showed that Ag ions are ferroelectrically active, and Shigemi and Wada, who examined the formation energies of different phases [14], using density functional theory (DFT). Niranjan and Asthana [15] later performed DFT calculations of the *Pbcm* and

Pmc2_1 structures proposed for the M_1 phase and found that there is only a tiny difference in energetic stability (≈ 0.1 meV/f.u.) between them, suggesting that under normal (room-temperature) conditions both are likely present in a polycrystalline material. Support for this interpretation has since been provided by Tian *et al.* [16] based on high-resolution electron microscopy images showing that at room temperature $AgNbO_3$ polycrystals consist of small polar domains with *Pmc*2_1 symmetry amidst larger non-polar domains with *Pbcm* symmetry. Additionally, Ahn *et al.* recently synthesized thin films of $AgNbO_3$ consisting of a mosaic of FE and AFE grains that exhibited an enhanced remanent polarization [17].

To shed greater light on the nature of the M1 phase, in an earlier paper [18] we reported first-principles calculations examining the phonon dispersion curves of FE and AFE single crystals. No soft-mode was found in the case of the AFE (M1-*Pbcm*) phase, indicating that it has a dynamically stable structure. Although lattice expansion is known to often stabilize ferroelectric phases, even under a large static tensile pressure, the M1-*Pbcm* phase remained dynamically stable. In contrast, the reported M1-*Pmc*2_1 structure spontaneously transformed into the M1-*Pbcm* structure upon geometry optimization (at 0 K). We concluded that the ferroelectric transition in $AgNbO_3$ cannot be described simply as a conventional first-order transition from high-temperature antiferroelectric phase to low-temperature ferroelectric phase.

DFT calculations of $AgNbO_3$ under an applied electric field showed that a fully FE structure, also belonging to space group *Pmc*2_1, and which we refer to as the F phase, becomes stable, with a theoretical polarization value of 61 μC/cm^2, in good agreement with the measured polarization under an applied electric field of 52 μC/cm^2 [19]. The F-*Pmc*2_1 structure is compared with M1-*Pbcm* and M1-*Pmc*2_1 structures in Fig. 1. These results suggest that, under an applied electric field, the F-*Pmc*2_1 structure forms the majority phase, whereas in the absence of an electric field the material exists as a mixture of

AFE domains (with *Pbcm* symmetry) and FE domains (with $Pmc2_1$ symmetry), resulting in an AFE-like *P-E* hysteresis loop with small remnant polarization (approx. 2 μC/cm^2).

To examine the dynamics of the FE-AFE phase transition and the role of structural fluctuations on phase stability in $AgNbO_3$ in more detail, we performed first-principles molecular dynamics simulations over a range of temperatures up to 400 K. Berry phase calculations of the mean polarizations of different structures and nudged elastic band calculations were then carried out to examine the FE-AFE transition mechanism in detail. We report results and interpretation of these calculations here, with the remainder of the paper structured as follows. In the next section we outline the principal simulation methods used, namely geometry-optimization within the framework of density functional theory, first-principles molecular dynamics simulations, and nudged elastic band and Berry phase calculations. In section 3 the results are presented and discussed in terms of the structural fluctuations at the microscopic level, and section 4 concludes the paper with a summary of the main findings.

2. Computational Procedure

All calculations were performed within the generalized gradient approximation, as developed by Perdew-Burke-Ernzerhof [20], within the framework of density functional theory (DFT) [21,22] using the plane-wave basis projector augmented wave (PAW) method [23]. The VASP code was used in all cases [24,25]. For the PAW potentials, 2*s* and 2*p* electrons for O; 4*s*, 4*p*, 4*d*, and 5*s* electrons for Nb; and 4*d* and 5*s* electrons for Ag were explicitly treated as valence electrons. Geometry optimization of the unit cells of the low-temperature AFE (*Pbcm*) structure and lower-temperature FE ($Pmc2_1$) structure was performed using a plane-wave cutoff energy of 550 eV and convergence criterion for residual forces of 0.01 eV/Å. A 3×3×2 ***k***-point mesh generated using the Monkhorst–Pack scheme [26] was used for both geometry optimization and MD calculations after confirming that energies converged to within 1

meV/atom up to a ***k***-point mesh of 8×8×3.

Supercells for MD simulations were constructed from 2×2×2 unit cells of the relaxed AFE (M1-*Pbcm*) structure and the electric-field stabilized FE (F-*Pmc*2_1) structure. Simulations were performed within the canonical ensemble (constant volume, temperature and number of atoms) at temperatures of 50, 100, 200, 300, and 400 K using a Nosé-Hoover thermostat [27] and an integration time step of 2 fs. The planewave cutoff for MD simulations was 400 eV. The canonical ensemble was chosen for studying FE-AFE transitions because the difference in lattice parameters (when the F-*Pmc*2_1 structure is converted to space group setting *P*2_1*am*) between the two forms at 0 K is less than 0.22 %. In each case, structures were relaxed for 1 ps (500 steps) to ensure thermodynamic equilibrium had been reached before performing production runs of 9 ps (4,500 steps).

Polarity switching frequencies for each structure at each temperature were calculated from the number of times the dipole moments of individual NbO_6 octahedra switched direction during the course of a simulation. Potential surfaces during polarization switching from AFE M1-*Pbcm* to FE F-*Pmc*2_1 structures were calculated using the nudged elastic band (NEB) method with a single unit cell at 0 K by incrementally shifting cations in half the crystal from AFE ordering to FE ordering. Mean polarizations at each temperature for each starting structure were calculated from averaged atom positions using the Berry phase method implemented in ABINIT [28]. Crystal structure analysis was performed using the VESTA code [29].

3. Results and Discussion

3.1 Polarity fluctuations at finite temperature

Figure 2a shows plots of polarity switching frequencies as a function of temperature for simulations commencing from either the AFE (M1-*Pbcm*) structure or the FE (F-*Pmc*2_1) structure.

Regardless of the starting structure, up to 100 K essentially no switches in polarity were observed. Between 100 K and 200 K, the frequency of switching increased slightly, and above 200 K it began to increase more rapidly. At 300 K and above, fluctuations between aligned octahedra and antiparallel octahedra were frequent, and it made little difference to the switching frequency whether systems commenced from the AFE or FE structure.

Plots of the net polarization of the crystal as a function of temperature commencing from the two structures are shown in Fig. 2b. At temperatures below 300 K, the F-$Pmc2_1$ structure retained its high polarization value, until at 300 K and above AFE regions formed for longer periods of time and the net polarization decreased, but did not entirely disappear. Similarly, at temperatures above 300 K, FE regions in the AFE crystal increased in size and duration.

Time-averages of atom positions during the course of each MD production run revealed that the mean displacement of Ag ions from the central perovskite site was smaller than that of the calculated F-$Pmc2_1$ structure at 0 K,[14] in good agreement with the room-temperature FE structure reported by Yashima *et al.*[4,5] These results demonstrate that formation of both phases is thermodynamically accessible at around 300 K, which is consistent with recent HRTEM observations by Tian et al.[25] of $AgNbO_3$ crystals consisting of a mixture of AFE and FE domains. This mixture of domains can explain the small remanent polarization typically reported from hysteresis loop measurements of $AgNbO_3$ polycrystals at room temperature.

3.2 Polarization switching mechanism

The polarization switching mechanism was analyzed in detail by plotting changes in Nb-O bond lengths and apical O-Nb-O bond angles of individual NbO_6 octahedra as a function of time at 400 K. An example is shown in Fig. 3. The two apical bonds of the octahedron in Fig. 3a oscillated about the same

mean value (≈ 2.0 Å; Fig. 3b) throughout the simulation, as did the corresponding apical angle (≈ 165°; Fig. 3c), indicating that no switches in polarity in the long-axis direction took place. In contrast, Figs. 3d and 3e show that the equatorial Nb-O bonds underwent step changes as a result of movement of the Nb atom from one side of the octahedron to the other within the equatorial plane, resulting in a reversal in polarity. These switches occurred rapidly, taking only a few femtoseconds.

An example of how a switch in polarity in a single octahedron relates to changes in polarization within one layer of the crystal as a whole is illustrated in Fig. 4a by snapshots of the structure at 400 K viewed down the long axis. Initially dipole moments of all NbO_6 octahedra within this one layer were oriented in the $+b$ direction, but by the end of the simulation they had collectively switched to the opposite direction after passing through an intermediate state with a mix of polarities. For example, as shown in Fig. 4a, after 5 ps, the mixed state had a small net polarization in the $+a$ direction.

Plots of the trajectories of Nb and O atoms (Fig. 4b) in the same layer as in Fig. 4a revealed that Nb atoms follow curved paths rather than straight paths when their octahedra switch polarity. Simultaneously, equatorial O atoms rotate slightly around the long octahedral axes, reaching the largest displacement before Nbs have reached the mid-points on their trajectories, before rotating back to their original sites. The MD results thus show directly that partial rotation of octahedra (according to constraints imposed by corner-sharing neighbors) plays an important role in the kinetics of ferroelectric switching in these perovskites.

Similar plots of Ag-O bonds within equatorial planes (Fig. S1 in the Supplemental Material [30]) and color-coded trajectories (Fig. S2 in the Supplemental Material [30]) revealed that while noticeable shifts in Ag-O bond lengths took place, the transitions were not as sharp as for Nb-O bonds, nor did they occur simultaneously with Nb switches, reflecting the more complex coordination environment and greater free volume of Ag sites, consistent with their much larger thermal factors from Rietveld analyses

at room temperature [2,4].

The energetics of the switching mechanism were probed by applying the NEB method to an antiferroelectric unit cell at 0 K. Potential surfaces were calculated during switching of the lower four octahedra and their neighboring Ag atoms in Fig. 1a from pointing in the $-b$ direction to the $+b$ direction via either a straight path or a curved path, and the results are plotted in Fig. 5 as a function of the normalized displacement of Nb atoms. The straight path produced a single maximum at the point midway between the initial and final states (when the Nb atom was midway between all four equatorial O), with an activation energy of 41 meV. In contrast, the curved pathway exhibited twin peaks, both with activation energies of only 19 meV, significantly lower than that for the straight path. It is worth noting that 19 meV is similar in magnitude to the thermal energy of vibrating atoms at room temperature, which explains the facile switching between FE and AFE structures at 300 K and above during MD calculations. The intermediate structure in this case has space group symmetry *Pm*, but phonon calculations showed that it is dynamically unstable and will transform to either the M1-*Pbcm* or F-$Pmc2_1$ structures at ambient temperature. The NEB calculations also confirmed the MD results indicating that polarity switching only occurs parallel to the equatorial plane, with little to no change in the long-axis direction. Piezoelectricity in $AgNbO_3$ single crystals is thus strongly anisotropic, which helps explains the large permittivities (≈500) observed experimentally [1], as each crystal is ferroelectrically inactive in the long-axis direction.

4. Conclusions

Systematic quantitative analysis of lattice fluctuations in $AgNbO_3$ at temperatures from 0 to 400 K was carried out using first-principles MD calculations within the framework of density functional theory. The main findings can be summarized as follows:

1) Polarity switching of NbO_6 octahedra started to occur from around 200 K but did not become significant until 300 K and above. Regardless of whether the starting structure was the antiferroelectric *Pbcm* phase or ferroelectric $Pmc2_1$ phase, above 300 K frequent switches in polarity corresponding to fluctuations between antiferroelectric and ferroelectric phases were observed. These periodic switches in symmetry confirm that both phases can form facilely below ~400 K, which may explain the coexistence of *Pbcm* and $Pmc2_1$ domains observed experimentally at room temperature. The MD results are also consistent with the experimentally observed room-temperature *P*-*E* hysteresis loop and crystal symmetries, and help explain the weak ferroelectric behavior of $AgNbO_3$ polycrystals.

2) During polarity switching, Nb ions follow a curved pathway within the equatorial plane of NbO_6 octahedra rather than a straight pathway parallel to the *b* axis, so that local polarization switching only occurs parallel to the short axes. Transition-state calculations using the NEB method estimated the activation energy for switching along a curved path to be 19 meV, less than half that for a straight path (41 meV), and comparable with thermal vibration energies at room temperature.

3) The anisotropy in polarization helps explain the large permittivities observed experimentally, as the single crystal is ferroelectrically inactive in one out of three directions.

Acknowledgments

This work was supported in part by Grant-in-Aid for Scientific Research on Innovative Areas "Nano Informatics" (grant number 25106008) from the Japan Society for the Promotion of Science (JSPS), and the Materials Research by Information Integration Initiative (MI^2I) project established with funding from the Support Program for Starting Up Innovation Hubs of the Japan Science and Technology Agency (JST).

References

1. D. Fu, M. Endo, H. Taniguchi, T. Taniyama, and M. Itoh, Appl. Phys. Lett. **90**, 252907 (2007).
2. Ph. Sciau, A. Kania, B. Dkhil, E. Suard, and A. Ratuszna, J. Phys., Condens. Matter **16**, 2795 (2004).
3. I. Levin, V. Krayzman, J. C. Woicik, J. Karapetrova, T. Proffen, M. G. Tucker, and I. M. Reaney, Phys. Rev. B **79**, 104113 (2009).
4. M. Yashima, S. Matsuyama, R. Sano, M. Itoh, K. Tsuda, and D. Fu, Chem. Mater. **23**, 1643 (2011).
5. M. Yashima and S. Matsuyama, J. Phys. Chem. C **116**, 24902 (2012).
6. H. Chang, M. Shang, C. Zhang, H. Yuan, and S. Feng, J. Am. Ceram. Soc., **95**, 3673 (2012).
7. H. Moriwake, C. A. J. Fisher, A. Kuwabara, and T. Hashimoto, Jpn. J. Appl. Phys. **50**, 09NE02 (2011).
8. H. Moriwake, C. A. J. Fisher, A. Kuwabara, H. Taniguchi, M. Itoh, and I. Tanaka, Phys. Rev. B **84**, 104114 (2011).
9. H. Taniguchi, H. P. Soon, T. Shimizu, H. Moriwake, Y. J. Shan, and M. Itoh, Phys. Rev. B **84**, 174106 (2011).
10. Y. Xu, G. Wang, Y. Tian, Y. Yan, X. Liu, and Y. Feng, Ceram. Intl. **42**, 18791 (2016).
11. T. Zhang, C. Zhang, L. Wang, Y. Chai, S. Shen, Y. Sun, H. Yuan, and S. Feng, J. Am. Ceram. Soc. **97**, 1895 (2014).
12. A. Paul, J. Sun, J. P. Perdew, and U. V. Waghmare, Phys. Rev. B **95**, 054111 (2017).
13. I. Grinberg and M. Rappe, *Fundamental Physics in Ferroelectrics 2003*, edited by P. K. Davis and D. J. Singh (American Institute of Physics, 2003), p.130.
14. A. Shigemi and T. Wada, Mol. Simul. **34**, 1105 (2008).

15. M. K. Niranjan and S. Asthana, Solid State Comm. **152**, 1707 (2012).

16. Y. Tian, L. Jin, H. Zhang, Z. Xu, X. Wei, E. D. Politova, S. Y. Stefanovich, N. V. Tarakina, I. Abrahams, and H. Yan, J. Mater. Chem. A **4**, 17279 (2016).

17. Y. Ahn, J. Seo, K. J. Lee, and J. Y. Son, J. Cryst. Growth **437**, 10 (2016).

18. H. Moriwake, C. A. J. Fisher, A. Kuwabara, and D. Fu, Jap. J. App. Phys. **51**, 09LE02 (2012).

19. H. Moriwake, A. Konishi, C. A. J. Fisher, T. Ogawa, A. Kuwabara, and D. Fu, J. Appl. Phys., **119**, 064102 (2016).

20. J. P. Perdew, K.Burke, and M. Ernzerhof, Phys. Rev. Lett. **77**, 3865 (1996).

21. P. Hohenberg and W. Kohn, Phys. Rev. **136**, B864 (1964).

22. W. Kohn and Sham, Phys. Rev. **136**, A1133 (1965).

23. P. E. Blöchl, Phys. Rev. B **50**, 17953 (1994).

24. G. Kresse and J. Furthmüller, Phys. Rev. B **54**, 11169 (1996).

25. G. Kresse and D. Joubert, Phys. Rev. B **59**, 1758 (1999).

26. H. J. Monkhorst and J. D. Pack, Phys. Rev. B **13**, 5188 (1976).

27. D. J. Evans and B. L. Holian, J. Chem. Phys. **83**, 4069 (1985).

28. X. Gonze, J.-M. Beuken, R. Caracas, F. Detraux, M. Fuchs, G.-M. Rignanese, L. Sindic, M. Verstraete, G. Zerah, F. Jollet, M. Torrent, A. Roy, M. Mikami, Ph. Ghosez, J.-Y. Raty, and D. C. Allan, Comput. Mater. Sci. **25**, 478 (2002).

29. K. Momma and F. Izumi, J. Appl. Crystallogr. **41**, 653 (2008).

30. See Supplemental Material at http:… for changes in Ag-O bond lengths as a function of time and trajectories of Ag, Nb, and equatorial O atoms.

Figure captions

Fig. 1 (Color online) Comparison of crystal structures of (a) M1-*Pbcm* (antiferroelectric), (b) M1-*Pmc*2_1 (ferroelectric), and (c) F-*Pmc*2_1 (ferroelectric) phases of $AgNbO_3$. Arrows indicate the relative magnitude and direction of atom displacement contributing the ferroelectricity (or lack thereof) in each structure.

Fig. 2 (Color online) (a) Polarity switching frequencies, and (b) mean polarizations calculated using the Berry phase method, at different temperatures from first-principles molecular dynamics simulations.

Fig. 3 (Color online) Structure changes in NbO_6 octahedra during molecular dynamics simulations at 400 K. (a) An ideal NbO_6 octahedron in orthorhombic $AgNbO_3$ with Nb-O bonds labeled 1 to 6; (b) Changes in Nb-O bond length for bonds 1 and 2; (c) Changes in Nb-O bond angle for bonds 1 and 2; (d) Changes in Nb-O bond length for bonds 3 and 4; (e) Changes in Nb-O bond length for bonds 5 and 6.

Fig. 4 (Color online) Polarization switching of one perovskite (in-plane) layer within $AgNbO_3$ at 400 K over 9 ps. (a) Snapshots of the Nb-O octahedra after 0 ps, 5 ps, and 9 ps viewed down the long axis. Arrows represent the direction and magnitude of polarization for each snapshot. (b) Trajectories of Nb and O atoms in the same layer as (a) color-coded according to the time scale shown above the plot. Dashed circles are aids for the eye to highlight the rotational arcs of equatorial O atoms in the Nb-O octahedra.

Fig. 5 (Color online) Calculated potential energy surfaces during polarization switching of $AgNbO_3$ from M1-*Pbcm* to F-*Pmc*2_1 structures. The inset illustrates the two pathways (straight and curved) used in the calculations for displacement of Nb within an NbO_6 octahedron in the *ab* plane.

Fig. 1

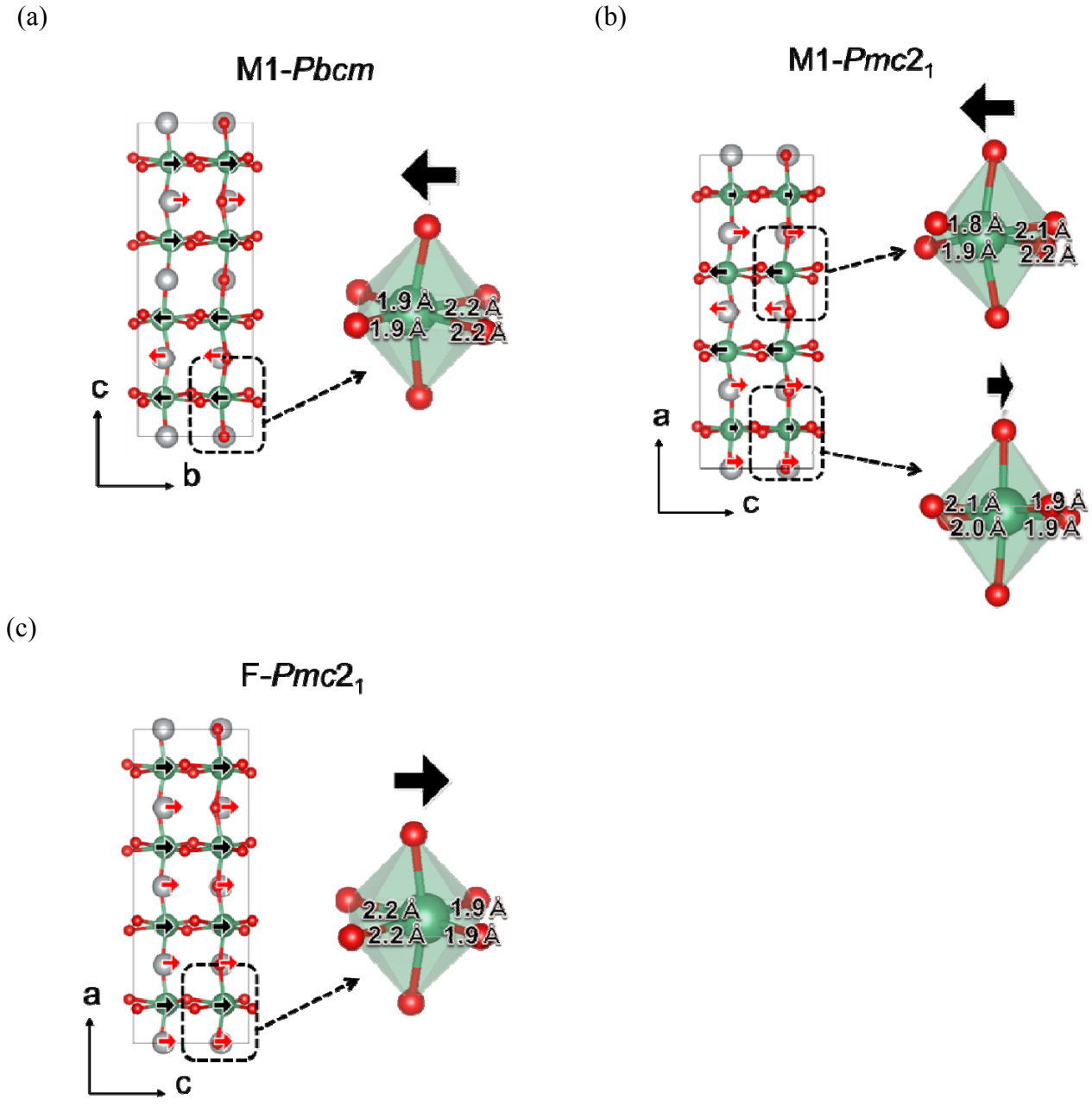
(a)
M1-Pbcm
1.9 Å
2.2 Å
1.9 Å
2.2 Å
c
b
(b)
M1-Pmc2$_1$
1.8 Å
2.1 Å
1.9 Å
2.2 Å
a
c
2.1 Å
1.9 Å
2.0 Å
1.9 Å
(c)
F-Pmc2$_1$
2.2 Å
1.9 Å
2.2 Å
1.9 Å
a
c

Fig. 2

(a)

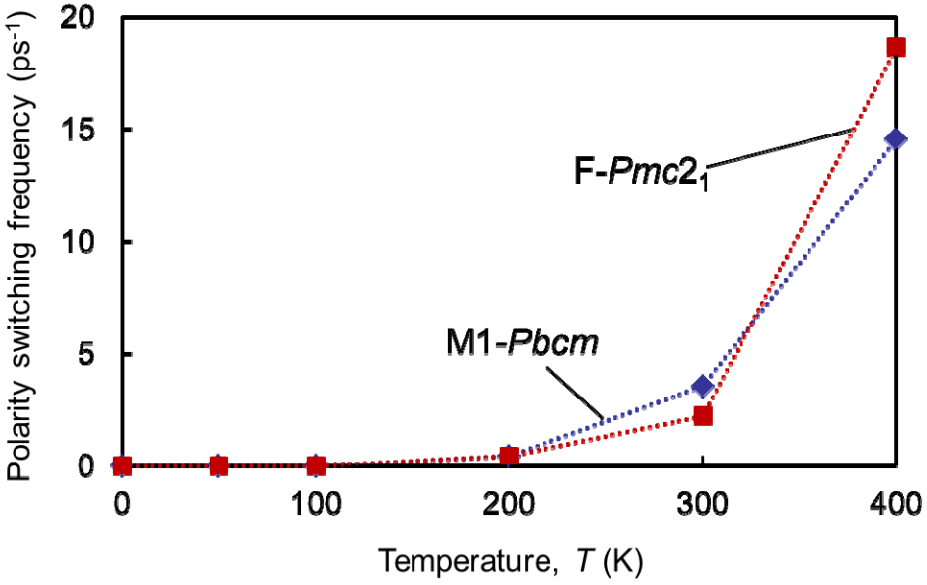
Polarity switching frequency (ps^{-1})
20
15
10
5
0
0
100
200
300
400
Temperature, T (K)
F-$Pmc2_1$
M1-$Pbcm$

(b)

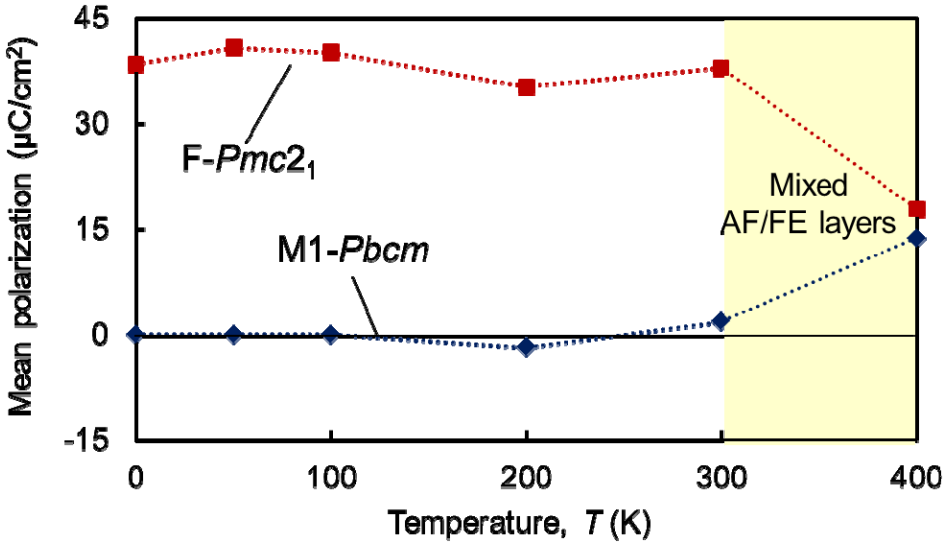
Mean polarization (μC/cm^2)
45
30
15
0
-15
0
100
200
300
400
Temperature, T (K)
F-$Pmc2_1$
M1-$Pbcm$
Mixed
AF/FE layers

Fig. 3

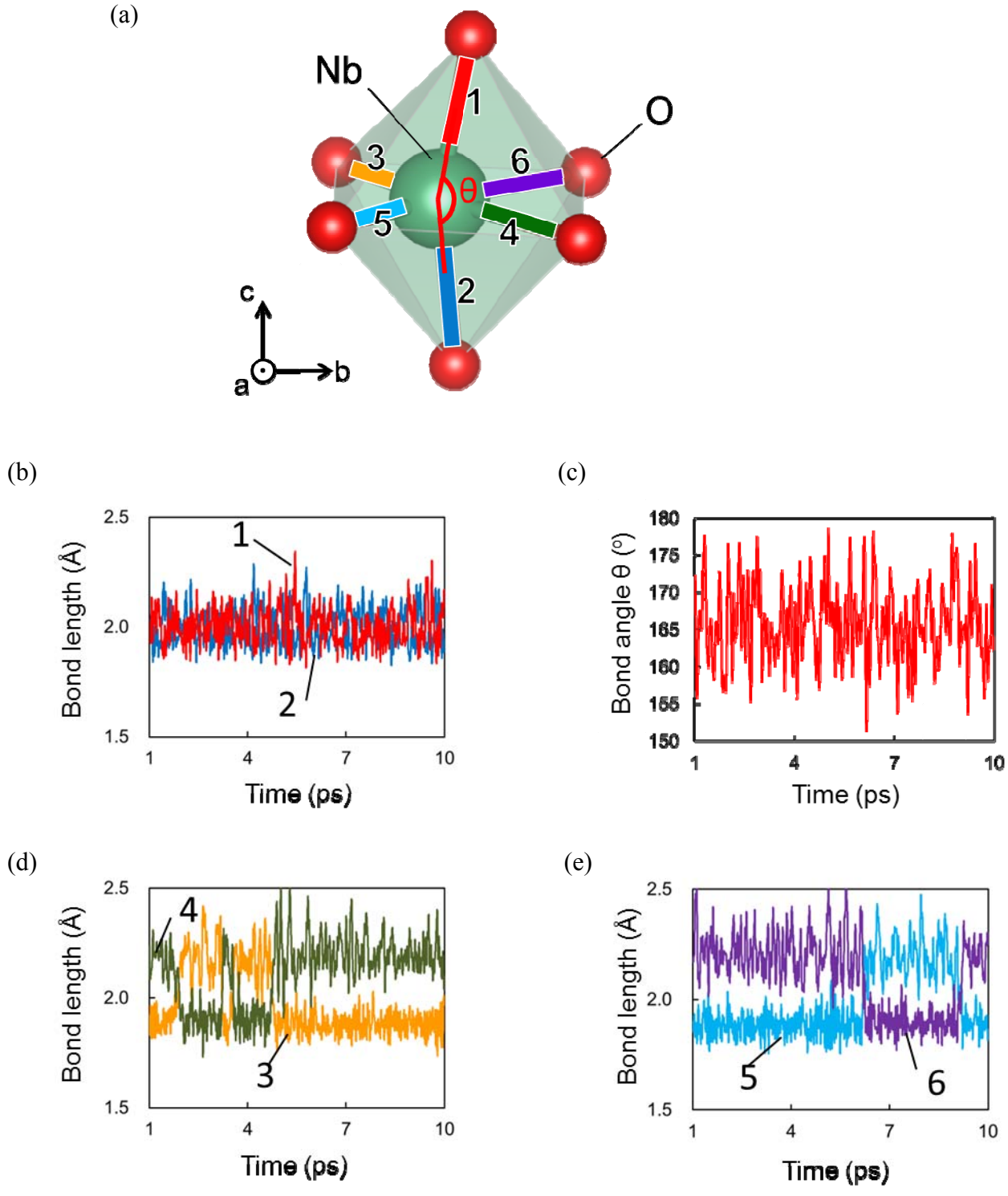
(a)
Nb
O
1
2
3
4
5
6
θ
c
a
b
(b)
Bond length (Å)
Time (ps)
(c)
Bond angle θ (°)
Time (ps)
(d)
Bond length (Å)
Time (ps)
(e)
Bond length (Å)
Time (ps)

Fig. 4

(a)

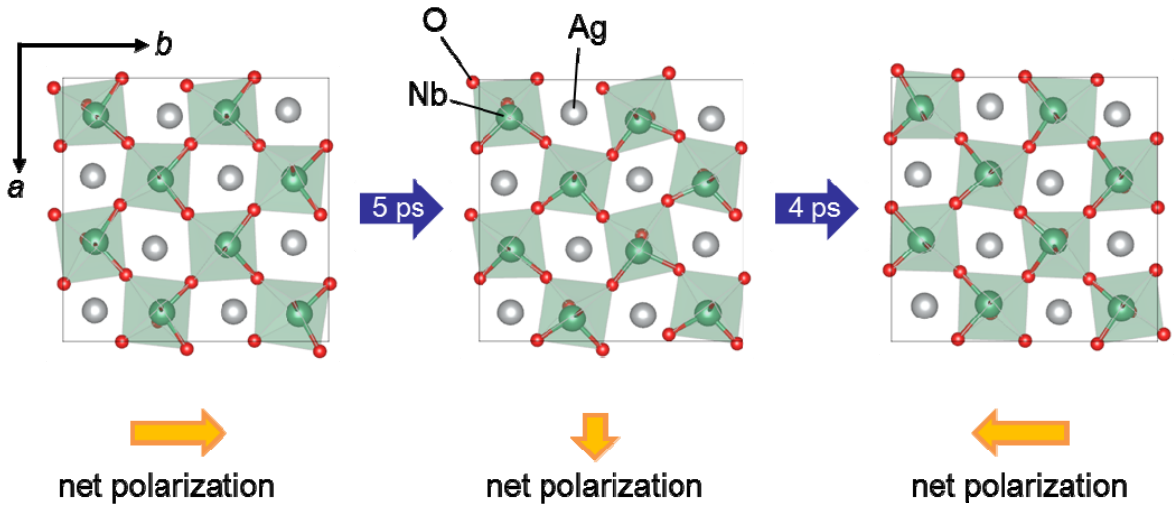
b
a
O
Ag
Nb
5 ps
4 ps
net polarization
net polarization
net polarization

(b)

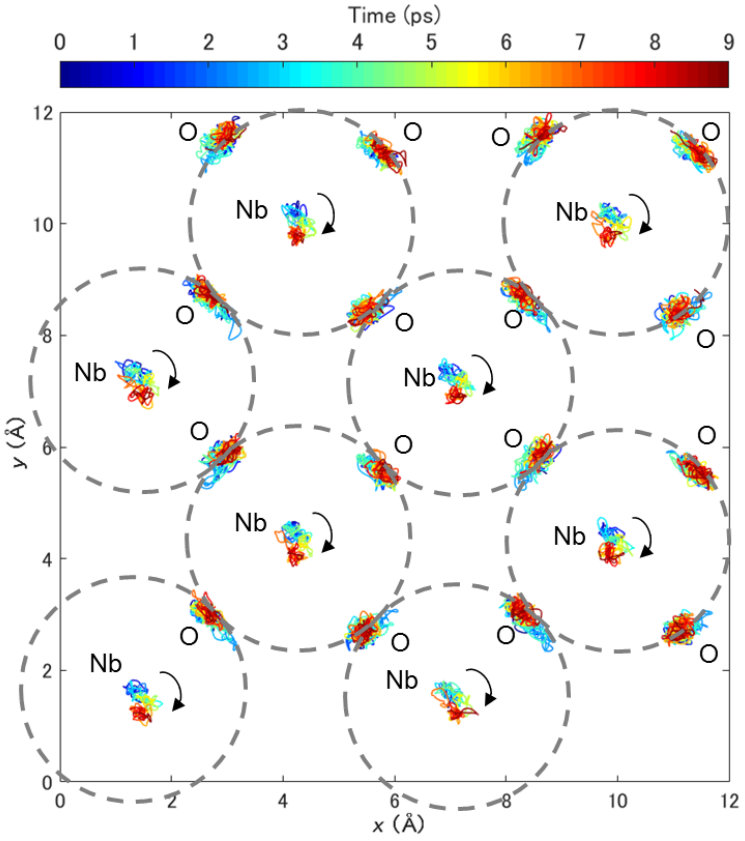
Time (ps)
0 1 2 3 4 5 6 7 8 9
O
Nb
y (Å)
x (Å)
0 2 4 6 8 10 12

Fig. 5

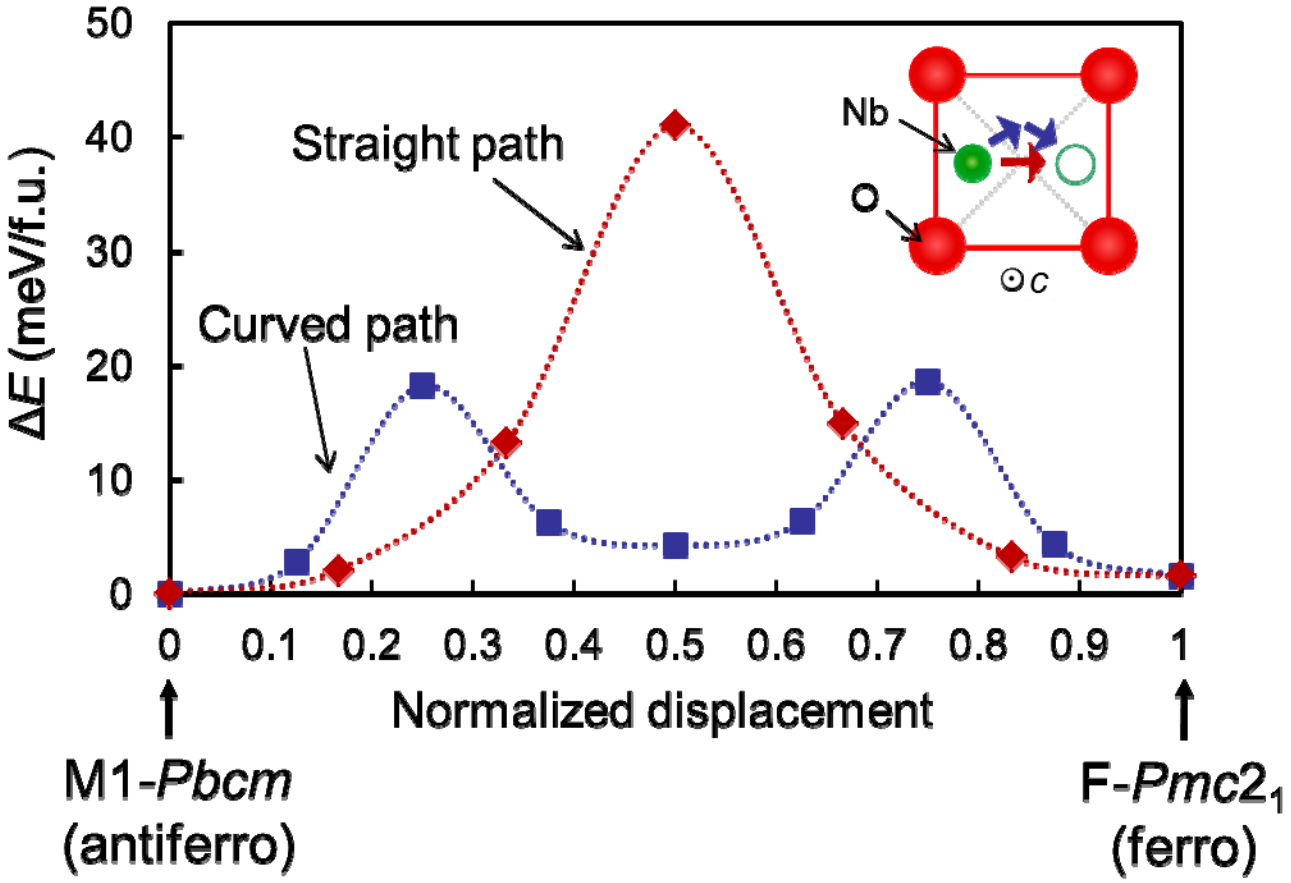
50
40
30
20
10
0
ΔE (meV/f.u.)
Straight path
Curved path
Nb
O
⊙c
0
0.1
0.2
0.3
0.4
0.5
0.6
0.7
0.8
0.9
1
Normalized displacement
M1-Pbcm
(antiferro)
F-Pmc2₁
(ferro)